Materials Today Advances 23 (2024) 100509

Contents lists available at ScienceDirect

Materials Today Advances

journal homepage: www.journals.elsevier.com/materials-today-advances/

3D printed electro-responsive system with programmable drug release

Manal E. Alkahtani [a,b], Siyuan Sun [a], Christopher A.R. Chapman [c], Simon Gaisford [a], Mine Orlu [a], Moe Elbadawi [d,**], Abdul W. Basit [a,*]

[a] UCL School of Pharmacy, University College London, 29-39 Brunswick Square, London, WC1N 1AX, United Kingdom
[b] Department of Pharmaceutics, College of Pharmacy, Prince Sattam Bin Abdulaziz University, Alkharj, 11942, Saudi Arabia
[c] Centre for Bioengineering, School of Engineering and Material Science, Queen Mary University of London, London, E1 4NS, United Kingdom
[d] School of Biological and Behavioural Sciences, Queen Mary University of London, London, E1 4NS, United Kingdom

ARTICLE INFO

Keywords:
On-demand drug release
Controlled release
Stimuli responsive drug delivery
Electrical stimuli
Electro-active polymers
Additive manufacturing
Semi-solid extrusion (SSE)
Direct ink writing (DIW)

ABSTRACT

Precision medicine is the next frontier in pharmaceutical research, aiming to improve the safety and efficacy of therapeutics for patients. The ideal drug delivery system (DDS) should be programmable to provide real-time controlled delivery that is personalised to the patient's needs. However, little progress has been made in this domain. Herein, we combined two cutting-edge technologies, conductive polymers (CPs) and three-dimensional (3D) printing, to demonstrate their potential for achieving programmable controlled release. A DDS was formulated where the CP provided temporal control over drug release. 3D printing was used to ensure dimensional control over the design of the DDS. The CP used in this study is known to be fragile, and thus was blended with thermoplastic polyurethane (TPU) to achieve a conductive elastomer with sound mechanical properties. Rheological and mechanical analyses were performed, where it was revealed that formulation inks with a storage modulus in the order of 10^3–10^4 Pa were both extrudable and maintained their structural integrity. Physicochemical analysis confirmed the presence of the CP functional groups in the 3D printed DDS. Cyclic voltammetry demonstrated that the DDS remained conductive for 100 stimulations. *in vitro* drug release was performed for 180 min at varying voltages, where a significant difference ($p < 0.05$) in cumulative release was observed between either ±1.0 V and passive release. Furthermore, the responsiveness of the DDS to pulsatile stimuli was tested, where it was found to rapidly respond to the voltage stimuli, consequently altering the release mechanism. The study is the first to 3D print electroactive medicines using CPs and paves the way for digitalising DDS that can be integrated into the Internet of Things (IoT) framework.

1. Introduction

Precision medicine is the next frontier in healthcare, aiming to precisely tailor therapeutic treatment to meet the patient's individual needs. Its importance arises from the recognition that traditional one-size-fits-all approach could cause variable treatment responses and outcomes. Despite the progress achieved in precision medicine, the toxicities and resistance of drugs remain significant challenges. The ideal medicine should factor in an individual's genetic makeup and accommodate their lifestyle habits [1]. Advances in precision medicine brought about high expectations for drug delivery systems (DDSs). Conventional DDSs suffer from safety, efficacy, and patient compliance issues caused by fluctuations in plasma drug levels, poor bioavailability, and repeated administration. Such challenges become more pronounced in chronic diseases that require long-term treatments. Controlled DDSs that release their drug load at the desired site and with specific dose on-demand are potential solution [2]. The development of such systems, which could be referred to as "smart", nowadays is increasingly becoming feasible due to the digital and technological advancement. Smart drug delivery systems (SDDSs) function by releasing their cargo in response to either (endogenous) internal stimulating signal such as plasma glucose levels, pH, redox state, and enzyme, or (exogenous) external stimulating signal, for example, ultrasound, temperature, magnetic, light, and electrical [3]. Among them, electrical stimulation has drawn considerable attention for various reasons including ease of control, repeated drug release, simple, and inexpensive [4]. Additionally, it can be easily integrated with sensors to provide closed-loop drug delivery and monitoring/diagnostic systems [5]. The system comprises

* Corresponding author.
** Corresponding author.
E-mail addresses: m.elbadawi@qmul.ac.uk (M. Elbadawi), a.basit@ucl.ac.uk (A.W. Basit).

https://doi.org/10.1016/j.mtadv.2024.100509
Received 16 February 2024; Received in revised form 14 June 2024; Accepted 21 June 2024
Available online 29 June 2024

an electric responsive carrier where drug(s) is loaded and uses electric field or current to stimulate and control drug release. Different types of drug release are achievable whether sustained over a period of time or pulsed in response to trigger. Overall, SDDSs have a broad applicability and can be developed as ingestible, injectable, implantable, or transdermal [6,7].

Recent advances in materials science have led to the development of smart electroactive biomaterials from which an electric responsive carrier for drug delivery can be made [8]. Different material types fall within this class including conductive polymers (CPs), metal/-semiconductors, and carbon-based materials. CPs are class of polymers that are intrinsically conductive with metal-like conductivity, yet offering the advantages of polymers that include processability, lightweight, chemical resistance and low cost [9]. There are around 25 CPs, of which those who have excellent electrical conductivity, good biocompatibility, and enhanced physical and chemical properties such as poly (3,4-ethyelenedioxythiophene) (PEDOT), polypyrrole (PPy), and polyaniline (PANi) are widely explored [10,11]. In healthcare, CPs have been used in biosensors, scaffolds for tissue engineering, actuators for artificial muscles, and drug delivery [4,9].

CPs have also been investigated as SDDS. To release their cargo, CPs undergo a series of conformational changes when electrically stimulated to release the drug by diffusion [4]. Another drug release mechanism could be oxidation or reduction reactions of the polymer caused by electrical stimulation that changes the polymer charge and repel oppositely charged drug molecule. These reactions are usually reversible, and CPs are responsive to repeated stimulations [5,12]. However, current fabrication methods suffer from limited resolution, high cost procedures and material wastage, which have hindered innovation [13].

Three-dimensional (3D) printing, or additive manufacturing, is a cutting-edge technology that transform computer created designs to unique objects in a layer-by-layer manner. Unlike traditional manufacturing processes, 3D printing is able to produce complex structures with high resolution. The technology allows rapid prototyping, and on-demand printing besides being cost effective and simple to operate [14–17]. Indeed, the versatility of the technology has prompted advances in several sectors. In the pharmaceutical field, a considerable amount of literature has been published showing the ability of 3D printing in the development of personalised dosage forms with different release profiles, geometries, and drug combinations [18–24]. The technology paved the way towards novel solutions to some of the major problems associated with traditional dosage forms including polypharmacy by fabricating 3D polypills [25,26], swallowing difficulties by producing orally disintegrating films/tablets or minitablets [27–31], and acceptability especially in children by creating chewable tablets with different shapes and flavours [32,33]. While intensive efforts have been devoted to 3D printing personalised medicines, only DDS with limited programmability have been achieved.

Here we investigate the potential of merging these two powerful technologies of CPs and 3D printing to achieve the next frontier of personalised medicines. The programmability of 3D printed electroactive DDS was evaluated using poly (3,4-ethylenedioxythiophene): polystyrene sulfonate (PEDOT:PSS) as the CP and loaded it with methylene blue as a model drug.

2. Materials and methods

2.1. Materials

Poly (3,4-ethylenedioxythiophene)-poly (styrenesulfonate) (PEDOT: PSS) (768,618-1G), dimethylsulfoxide (DMSO), dimethylformamide (DMF), and methylene blue (MB) (M9140-25G) were obtained from Sigma Aldrich (Gillingham, UK). Thermoplastic polyurethane (TPU) (ElastollanR) was received from BASF (Ludwigshafen, Germany). Deionized water was generated using ELGA water purification system (VWS Ltd., UK). Phosphate-buffered saline (PBS) (pH = 7.4) was prepared using 8.0 g/L NaCl, 0.2 g/L KCl, 1.42 g/L Na_2HPO_4 and 0.24 g/L KH_2PO_4, all of which were also purchased from Sigma Aldrich (Gillingham, UK).

2.2. Feedstock preparation

CP inks were prepared by dissolving PEDOT:PSS into DMF at specific quantities (Table 1) and mixing using a hot plate stirrer at 400 rpm and at room temperature for 12 h. Once dissolved, TPU pellets were then added to the solution and were further mixed at a temperature of 80 °C until a homogenous solution was obtained. Following this, MB was introduced into the solution and was mixed for an extra 1 hour. A total of 11 inks were prepared and analysed using a rotational rheometer. After a preliminary screening of printability for a series of solvents, suitable inks were then selected and stored in closed vials until ready for 3D printing.

2.3. 3D printing procedure

A computer-aided design (CAD) software (Onshape Inc., Boston, MA, USA) was used to design the film model. Films were designed with a length, width and thickness of 20.00, 10.00 and 0.25 mm, respectively. Thereafter, the designs were exported as a. stl file and uploaded onto the BioX, a direct ink writing (DIW) printer (Cellink, Gothenburg, Sweden).

CP inks were loaded into 3 mL syringes compatible with the printer and subsequently fitted with 27 G nozzles. The syringes were then attached to the printer's compressed air line. Samples were printed on a petri dish that was lined with a Baseboard's Painter's Tape #2093 EL to facilitate the adhesion of the prints, and the subsequent detachment. After a series of trial-and-error, an ideal parameter set was established (Table 2). The printed films were left to dry for 48 h at ambient conditions, which were then used for further analysis.

2.4. Characterisation

2.4.1. Rheology

The rheological analysis was carried out using Bohlin Gemini HR Nano (Malvern Instruments, Malvern, UK) to study the materials viscoelastic behaviour. An oscillation test was selected to measure elastic (storage) modulus (G′) for 7 min, following an amplitude sweep to determine the linear viscoelastic region, where 7 min was the time it took for printing. A 20 mm diameter parallel plate was used, and the gap distance was set to 500 μm. The shear frequency was set to 1 rad/s with a shear stress of 10 Pa. Other test parameters included a controlled shear rate of 0.1 s^{-1} and shear frequency of 1 rad/s.

2.4.2. Film physical properties

The dried film weight was determined using analytical balance (Sartorius AG CPA225D, Germany) and a weighing boat. Film thickness was measured at various locations on the film using digital calliper D03196 (DuraTool, Taichung, Taiwan). The dimensions were measured

Table 1
Compositions of the formulations used as ink for printing.

Formulation	PEDOT: PSS (w/v)	TPU (w/v)	DMF (% v/v)	MB (w/v)
1	1 %	–	100	1 %
2	2 %	–	100	1 %
3	3 %	–	100	1 %
4	4 %	–	100	1 %
5	5 %	–	100	1 %
6	4 %	1 %	100	1 %
7	4 %	2 %	100	1 %
8	4 %	3 %	100	1 %
9	4 %	4 %	100	1 %
10	4 %	5 %	100	1 %
11	4 %	6 %	100	1 %

Table 2
Optimised 3D printing parameters.

3D printing parameters	
Needle gauge (Needle diameter)	27G (0.2 mm)
Compressed air pressure	70 kPa
Printing speed	20 mm/s
Infill pattern	Grid infill
Infill density	50 % Feedstock
Temperature	20-25 °C
Humidity	35–45 %

using a ruler. The data represent the mean and ±SD of at least three replicates.

2.4.3. Differential scanning calorimetry (DSC)

DSC was used to characterise and compare different 3D printed films, and the as-received PEDOT:PSS, TPU and MB. The analysis was conducted using Q2000 DSC (TA instruments, Waters, LLC, New Castle, DE, USA); while TA Advantage software for Q series (version 2.8.394, TA instruments, Waters LLC, New Castle, DE, USA) and TA Instruments Universal Analysis 2000 were used to collect and analyse the data, respectively. Samples with an average mass of 5 ± 0.5 mg were placed in aluminium pans with pin-holed hermetic lids (T_{zero}). For all experiments, nitrogen was used as a purge gas with a flow rate of 50 mL/min. The samples were equilibrated at 30 °C then were heated to 200 °C at a rate of 10 °C/min. OriginPro® 2021 software (OriginLab Corporation, Northampton, MA, USA) was used to plot and analyse the data.

2.4.4. Raman spectroscopy

As-received samples of MB, PEDOT:PSS, and TPU, and 3D printed samples of PEDOT:PSS/TPU films with and without MB were evaluated using inViaTM confocal Raman microscope (Renishaw, UK). A 20× objective lens was used to focus the 532 nm laser. Once focused, an extended grating scan was performed from 2000 to 100 cm^{-1} with an exposure time of 10 s. OriginPro® 2021 software (OriginLab Corporation, Northampton, MA, USA) was used to plot and analyse the spectra.

2.4.5. X-ray diffraction (XRD)

The physical state of the 3D printed films and as-received starting materials were analysed using MiniFlex 600 benchtop diffractometer (RigaKu, Tokyo, Japan) with a Cu Kα X-ray source (λ = 1.5418 Å). The voltage and current used in the analysis were 40 kV, and 15 mA, respectively. The X-ray diffraction patterns were recorded over 2θ range between 3° and 60°, with a step size of 0.02° and at a scan speed of 10°/minute. OriginPro® 2021 software (OriginLab Corporation, Northampton, MA, USA) was used to plot and analyse the XRD patterns.

2.4.6. Electrical stability

Cyclic voltammetry (CV) was used to study the electrical stability of both PEDOT:MB and PEDOT:TPU:MB films. CV was carried out using a three-electrode setup, electrolyte media, and a potentiostat. A platinum mesh (Goodfellow Cambridge Ltd., UK) and Ag/AgCl wire (BASi Inc., West Lafayette, IN, USA) was used as counter electrode and reference electrode, respectively. The 3D printed devices were attached to the working electrode. PBS was used as the electrolyte solution not only because it is conductive but also it simulates biological fluids. It was prepared freshly by dissolving 8 g sodium chloride (NaCl), 0.2 g potassium chloride (KCl), 0.24 g dipotassium hydrogen phosphate (K_2HPO_4), and 1.44 g disodium phosphate (Na_2HPO_4) in 1 L of distilled water; the pH was adjusted to 7.4. A PalmSens4 potentiostat (Palmsens BV, Houten, Netherlands) was used and the test was set up at a scan rate of 0.5 V/s with a step of 0.005 V. A total of 100 cycles were conducted within −0.5 to +0.5 V. OriginPro® 2021 software (OriginLab Corporation, Northampton, MA, USA) was used to plot and analyse the cyclic voltammograms.

2.4.7. Dynamic mechanical analysis (DMA)

The mechanical properties of 3D printed conductive elastomers with and without MB were analysed using Q800 DMA (TA Instruments, USA). Each rectangular film was measured for their width and thickness using a Vernier calliper. Samples were then attached to the tensile clamps, and the length of the measurement area was recorded. Samples were loaded at a displacement rate of 500 μm/min. OriginPro® 2021 software (OriginLab Corporation, Northampton, MA, USA) was used to plot and analyse the data; experiments were performed in triplicate and the data were reported as mean value ± SD.

2.4.8. In vitro drug release study

For the passive release test, the MB-loaded films were placed in a flask with 50 mL of PBS (pH 7.4). At predetermined time intervals, 1 mL of the release solution was withdrawn and replaced with 1 mL of the fresh buffer to maintain constant volume. The amount of drug released was determined with Cary 100 UV–vis spectrophotometer (Agilent Technologies, UK) operated at 664 nm detection wavelength. A calibration curve using MB and PBS as the media was developed to quantify the cumulative MB release. The voltage-driven release test was achieved using a three-electrode system consisting of the 3D printed film as working electrode, a platinum mesh counter electrode (Goodfellow Cambridge Ltd., UK) and an Ag/AgCl wire reference electrode (BASi Inc., West Lafayette, IN, USA) in 50 mL of PBS. Different voltages (−0.5, −1.0, +0.5 and +1.0 V) were applied to study the electric-driven release behaviour. To further explore the films' electric-driven release behaviour, an "on–off" pulse release method was employed. Specifically, the films were exposed to three +1.0 V voltage pulses for a total of 2.5 min per pulse, with a 5.0 min "off" period in between. The amount of drug released from the films was calculated using the aforementioned method.

2.4.9. Swelling test

To evaluate the swelling behaviour of 3D printed films, a swelling test was conducted using PBS (pH 7.4). The MB-loaded conductive elastomer films were initially weighed using an analytical balance (Sartorius AG CPA225D, Germany) to determine their initial dry weight (W_0). Each film sample was then placed in a beaker containing 50 mL of PBS solution and incubated at 37 °C for 3 h to simulate release study conditions. After the incubation period, the films were removed from the solution, gently blotted with tissue to remove excess PBS, and immediately weighed to obtain the wet weight (W_1). The swelling ratio for each sample was calculated using the equation:

$$\textit{Swelling ratio}\ (\%) = \frac{W_1 - W_0}{W_0}\ \text{x}\ 100 \quad (1)$$

This procedure was repeated in triplicate to ensure reproducibility.

2.4.10. Scanning electron microscopy (SEM)

The surface morphology of the printed films both before and after electrical stimulation were examined using FEI Quanta 200 FEG SEM (FEI, Hillsboro, OR, USA). The films were first mounted on carbon adhesive discs that were fixed onto aluminium stub. Thereafter, they were sputter coated with gold (25 nm). The images were captured at an accelerating voltage of 5.0 kV.

2.5. Statistical analysis

All experiments were performed in triplicate and the data were presented as mean value ± SD. OriginPro® 2021 software (OriginLab Corporation, Northampton, MA, USA) was used to statistically analyse the data. To compare drug release data, one-way repeated measures ANOVA was applied, followed by Tukey's pairwise comparison test ($p < 0.05$). In addition, the f_2 similarity factor was also implemented:

$$f_2 = 50 \cdot log\left\{\left[1 + \frac{1}{n}\sum_{t=1}^{n}(R_t - T_t)^2\right]^{-0.5} \times 100\right\} \quad (2)$$

where n is the number of time points, R_t is the mean release percentage at time point t for the reference profile, and T_t is the mean release percentage at time point t for the test sample. All time points were used for the calculation. The passive release (i.e., 0V) was used as the reference profile when compared to. A release profile is considered dissimilar if the factor value is below 50 [34]. The f_2 similarity factor was used because it is a standardised test recommended by the FDA for comparing dissolution profiles. Compared to ANOVA, the f_2 similarity factor considers time as a function, rather than treating the individual time points as separate groups.

3. Results

3.1. Rheological characterisation of feedstock

PEDOT:PSS is known to be mechanically fragile, and thus the initial objective was to formulate it such that it can lead to a product with adequate mechanical properties. As PEDOT:PSS is inherently brittle, it was blended with a common elastomer, TPU, to impart flexibility and to counteract the brittleness (Fig. 1 (a)). Subsequently, the aim was to formulate the new polymer blend such that it was amenable to 3D printing (Fig. 1 (b)). Previous work has reported the challenges in achieving printable PEDOT:PSS inks, with incremental increases of polymer loading (i.e., 1 w/v%) affecting printability [35]. Thus, we set out to determine the printability of our bespoke PEDOT:PSS inks prior to blending with TPU.

DMF was chosen as the solvent for this study, as it can dissolve both PEDOT:PSS and TPU. It was possible to dissolve PEDOT:PSS up to 5 w/v %, whereas 6 w/v% PEDOT:PSS loading resulted in an inhomogeneous admixture. An initial attempt to print the inks revealed different printing characteristics when the polymer loading was varied. Both the 1 and 2 w/v% polymer loadings resulted in over extruded formulations that spread shortly after being extruded from the nozzle (Fig. S1). In contrast, 5 w/v% polymer loading resulted in under-extruded films, characterised by voids and incomplete printing of the desired CAD model (Fig. S1). Inks with either 3 or 4 w/v% polymer loading were found to print the desired structure, with inks maintaining their structural integrity. Rheological characterisation was performed to quantify the printability of these inks. The analysis revealed that increasing the polymer loading from 1 to 2 w/v% had a marked increase in the elastic modulus (G′), from 10^{-2} to 10^{2} Pa (Fig. 1 (c)). Further increases to the polymer loading resulted in less pronounced increases to the G′, where the G' at 5 w/v% was in the order of 10^{3} Pa. Thus, we were able to quantify the printability window of the PEDOT:PSS inks (Fig. 1 (d)). Furthermore, the rheological analysis also revealed that the inks were rheologically stable for 7 min, with no evidence of thixotropic nor rheopectic behaviour.

While both 3 and 4 w/v% resulted in printable inks that were able to maintain their structural integrity, it was decided to blend TPU with the higher concentration, in order to maximise the conductivity of the final product. TPU loading was incrementally explored from 1 to 6 w/v%. At 4 w/v% PEDOT:PSS, the addition of 1 w/v% TPU was found to increase the G′ to 10^{3} Pa, whilst adding 6 w/v% TPU yielded the highest G' value, which was in the order of 10^{4} Pa (Fig. 1 (e)). Attempts to print these inks were successful at 4 w/v% PEDOT:PSS whilst varying the TPU loading between 1 and 6 w/v%, insofar as the films maintained their structural integrity. However, only solutions containing 6 w/v% TPU were found to be ductile and workable after drying. These films were stretched, bent and twisted without fracturing, thereby demonstrating their ductility (Fig. 1 (f)). Therefore, our empirical tests revealed that the optimal formulation comprised 6 w/v% TPU and 4 w/v% PEDOT:PSS.

3.2. Physico-chemical characterisation of 3D printed films

As mentioned in the Introduction, 3D printing offers high dimensional accuracy and precision. The physical properties with respect to weight and dimensions were also recorded and are presented in Table 3. The films were designed with dimensions of 20 mm length by 10 mm width by 0.25 mm thickness on the CAD software (Fig. 1 (b)). It was observed that the length and width were fabricated with high accuracy and precision. For example, the PEDOT:PSS/TPU/MB films deviated by

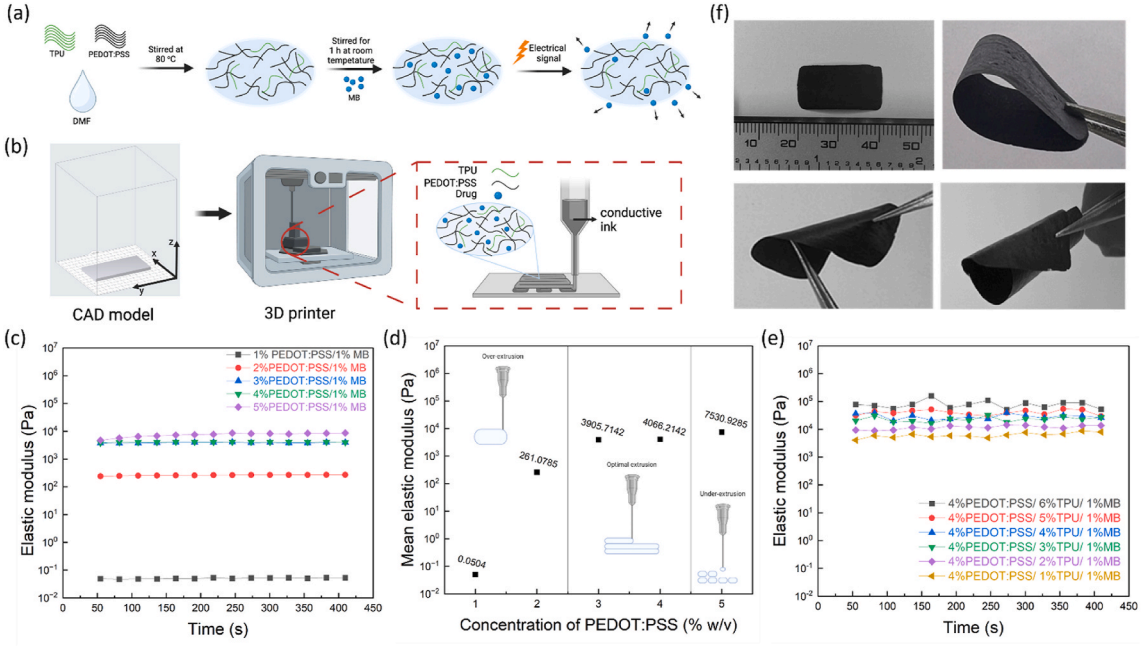

Fig. 1. (a) Schematic illustration of conductive ink preparation process showing the drug release upon application of electrical stimulus in an electro-responsive system; (b) schematic illustration showing the 3D printing process and the composition of the conductive ink; (c) rheological profiles of various concentrations of PEDOT:PSS/MB formulations; (d) mean elastic modulus as a function of PEDOT:PSS concentration; (e) rheological profiles of various concentrations of PEDOT:PSS/TPU/MB formulations; and (f) images of the 3D printed conductive film as intact, undergoing stretching, bending, and twisting without fracturing or damage.

Table 3
The mean weight, thickness, and dimensions of the PEDOT: PSS and PEDOT: PSS/TPU films (n = 3).

Film type	Weight (mg) (mean ± SD)	Thickness (μm) (mean ± SD)	Dimensions (mm) (mean ± SD)	
			Length	Width
PEDOT:PSS/MB Film	18 ± 0.10	47.2 ± 0.20	18.6 ± 0.34	9.6 ± 0.57
PEDOT:PSS/TPU/MB Film	19.36 ± 1.58	41 ± 0.01	20.05 ± 0.04	10.05 ± 0.05

0.05 mm for both length and width. The thickness on the other hand was 0.047 mm, which is notably different to the CAD design, and could be attributed to the sample evaporation. If so, then it suggests that axial evaporation had occurred as the length and width maintain their dimensional accuracy. Nevertheless, the measurements confirmed that 3D printing yields films with consistent physical features.

A range of characterisation was performed to provide further insight into the conductive elastomer (Fig. 2). The starting materials were mixed at 80 °C to facilitate mixing, and DSC analysis confirmed that the starting materials (i.e., PEDOT:PSS, TPU and MB) were thermally stable up to 80 °C, with no evidence of thermal events observed until 120 °C in both PEDOT:PSS and MB (Fig. 2 (a)). A sharp exothermic peak was observed for the raw MB, which was attributed to its degradation. The DSC also confirmed that the films were successfully evaporated, with no exothermic peak indicating the presence DMF.

All three starting solid materials contain functional groups that are amenable to vibrational analysis (Fig. 2 (b)) and thus attenuated total reflectance Fourier transformed infrared (ATR-FTIR) spectroscopy was employed to elucidate the chemical structure for both the starting materials and films. While the analysis was able to characterise the raw TPU and MB, as well as confirming their presence within the 3D printed films (Fig. S2), there was difficulty in characterising PEDOT:PSS, potentially due to the electrostatic interference when the polymer comes into contact with ATR-FTIR crystal. It was not possible to discern the peaks of the raw PEDOT:PSS pellets, whilst films containing the polymer resulted in baselines offsets at the fingerprinting region (Fig. S2). As a result, Raman spectroscopy was employed to confirm the presence of PEDOT:PSS (Fig. 2 (c)). The analysis of the PEDOT-only film revealed the presence of PEDOT and PSS functional groups, in accordance with previous work [36,37]. A characteristic peak of PEDOT was detected around 1450 cm^{-1}, which is associated with the C═C stretching mode of the thiophene rings. Minor peaks pertaining to PEDOT were also detected at 580 and 720 cm^{-1}, which were associated with the bending modes of the thiophene rings in PEDOT. The peak at 1000 cm^{-1} was associated with the stretching mode of the S═O bonds in the PSS component. Such peaks were observed in the PEDOT:PSS/TPU/MB films, albeit at a lower intensity. Furthermore, a prominent peak located at 1625 cm^{-1} was observed, which is associated with C═C stretching mode of the aromatic ring of MB [36,37].

XRD analysis was conducted (Fig. 2 (d)), where the diffractogram for the raw PEDOT and TPU presented with a broad halo, confirming that both polymers were amorphous. The raw MB powder was found to possess several peaks, revealing that it was crystalline. The MB peaks were in agreement with previous work [38]. However, these peaks were not evident in the PEDOT:PSS/TPU/MB films, inferring that the MB was molecularly dispersed within the films [39].

The analyses from Fig. 2 indicated that the PEDOT:PSS was unperturbed after being subjected to high temperatures during mixing, as well as subjected to shearing during 3D printing. The conductivity of the 3D printed films was then investigated using cyclic voltammetry (CV), as depicted in Fig. 3 (a). The conductivity of the PEDOT:PSS films with MB were compared to films containing TPU, where the analysis revealed

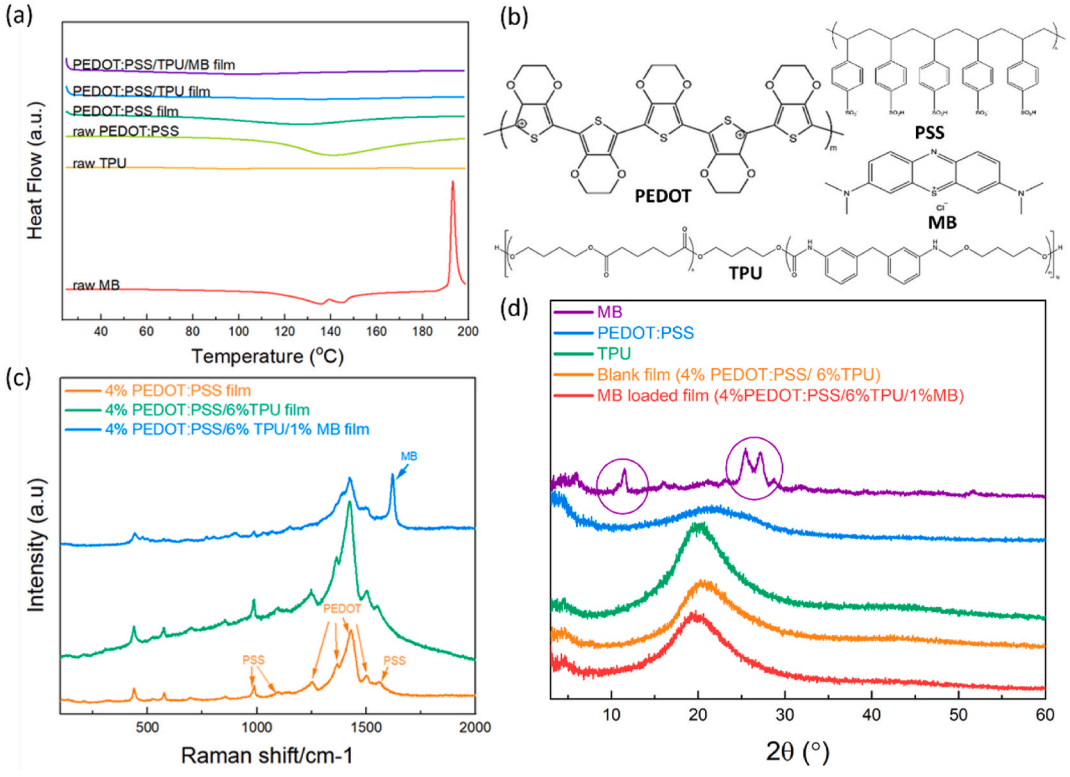

Fig. 2. (a) DSC thermograms of raw methylene blue (MB), raw thermoplastic polyurethane (TPU), raw poly (3,4-ethylenedioxythiophene)-poly (styrenesulfonate) (PEDOT: PSS), PEDOT:PSS film, PEDOT:PSS/TPU film, PEDOT:PSS/TPU/MB film; (b) chemical structures of PEDOT, PSS, MB, and TPU; (c) Raman spectra of PEDOT: PSS film, PEDOT:PSS/TPU film, PEDOT:PSS/TPU/MB film; and (d) X-ray diffractograms of raw MB, raw PEDOT:PSS, raw TPU, PEDOT:PSS/TPU film, and PEDOT: PSS/TPU/MB film. (For interpretation of the references to colour in this figure legend, the reader is referred to the Web version of this article.)

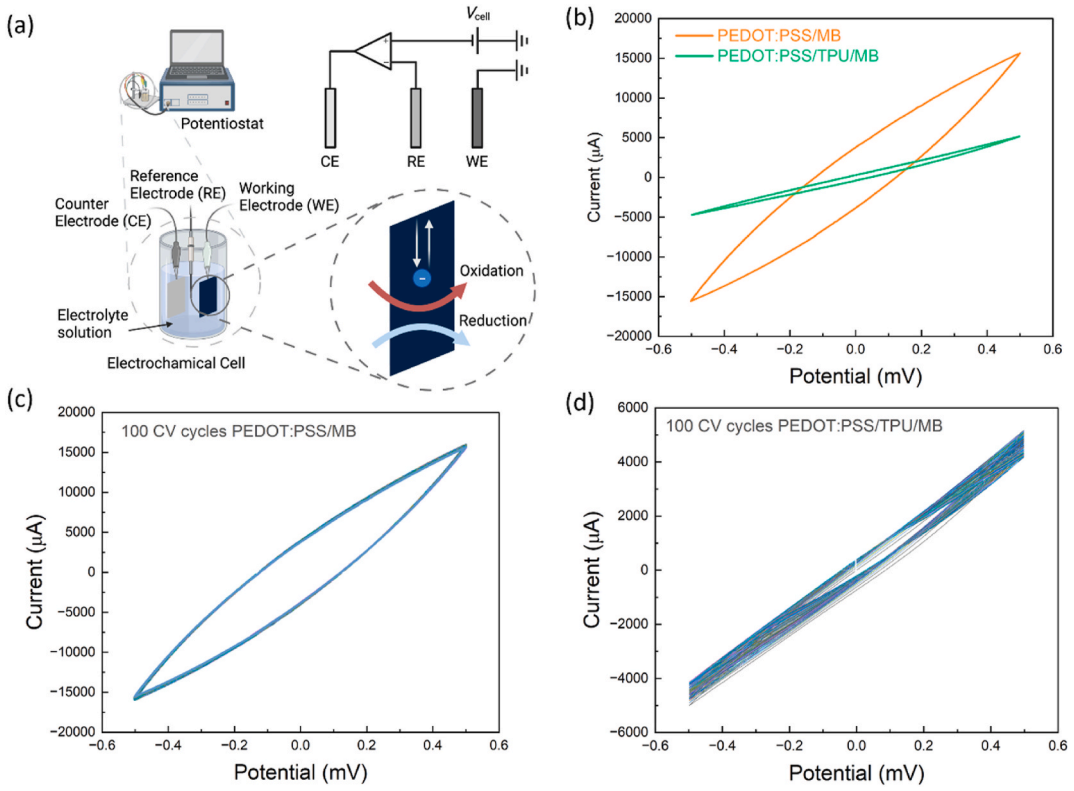

Fig. 3. (a) Schematic illustration of the electrochemical setup, consisting of a three-electrode system connected to a computer-controlled potentiostat; (b) cyclic voltammograms (CV) of PEDOT:PSS/MB film and PEDOT:PSS/TPU/MB film; (c) 100 CV cycles of PEDOT:PSS/MB film; and (d) 100 CV cycles of PEDOT:PSS/TPU/MB film.

that the peak currents were 15.96 and 5.18 mA, respectively (Fig. 3 (b)). Thus the CV confirmed that both films were conductive, whilst the addition of 6 w/v% TPU resulted in a decrease in peak current by 67.54 %. Additionally, the electrical stability of both films was assessed by performing 100 CV cycles. The hysteresis loop of PEDOT:PSS/MB presented with marginal deviation over 100 cycles, as depicted in Fig. 3 (c).

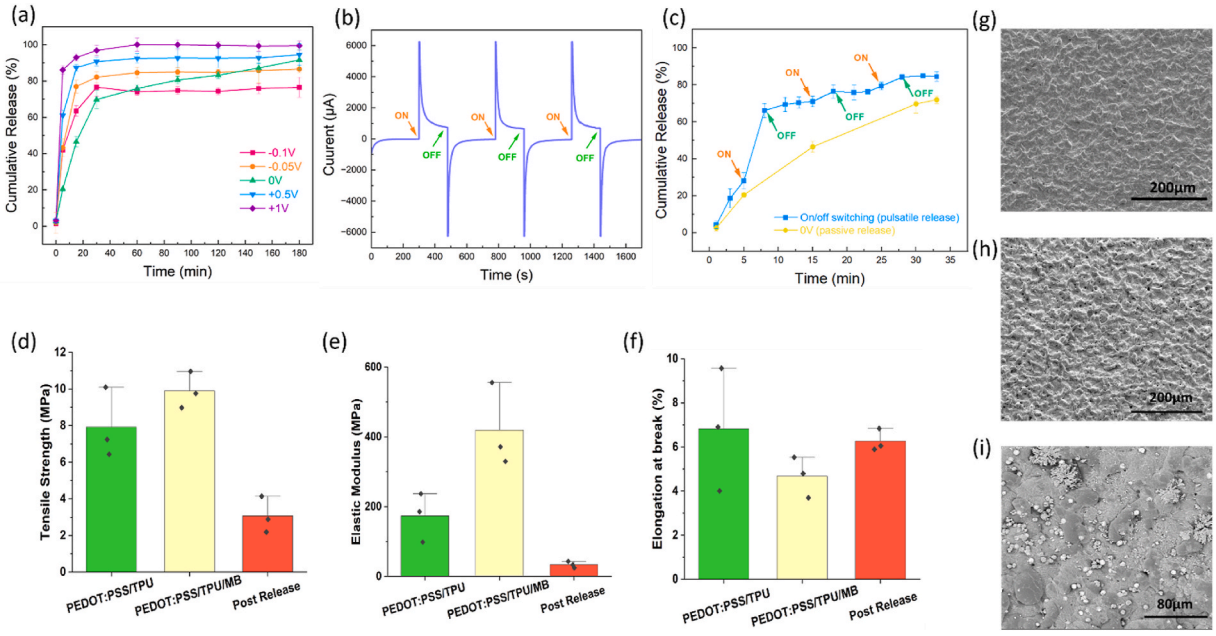

Fig. 4. (a) MB cumulative release profiles upon stimulation at −1.0, −0.5, +0.5, or +1.0 V and without stimulation (0.0 V). f_2 similarity factor confirmed statistically significant differences in release profiles. (b) current-time response during chronoamperometry experiment. (c) MB pulsatile release profile with on/off switching compared to passive release (0.0 V). (d–f) the tensile properties of the conductive elastomer with respect to their tensile strength, elastic modulus and elongation at break, respectively. The post release films were those subjected to +1.0 V for 180 min. (g–i) SEM images of PEDOT:PSS/TPU/MB films after release experiments with passive, +0.5 and + 1.0 V, respectively.

By the end of the 100th cycle, the peak current decrease from 15.96 to 15.22 mA, which is a decrease of 4.64 %. The peak current for the PEDOT:PSS/TPU/MB at the 100th cycle was recorded at 4.18 mA, which was a decrease of 19.30 % (Fig. 3 (d)). In other words, these films maintained 80.70 % of their initial conductivity after 100 CV cycles (Fig. S3).

3.3. In vitro analysis

In vitro dissolution was performed to determine whether the conductive elastomer can modulate drug release. The release of MB from the PEDOT:PSS/TPU/MB films was tested in PBS media and at voltages ranging from −1.0 to +1.0 V, including a passive release at 0.0 V. MB is a positively charged drug and thus is expected to respond to voltage stimuli. The drug release was monitored for 180 min, where it was discovered that various release profiles were obtained as the voltage was changed (Fig. 4 (a)). The voltage-stimulus, whether positive or negative, resulted in an initial burst release compared to the passive films. At 30 min, the mean cumulative release for +1.0, +0.5, −0.5 and −1.0V were 96.82 ± 2.91 %, 90.63 ± 2.39 %, 81.10 ± 3.02 % and 76.56 ± 4.99 %, respectively. This ranking order was maintained until the end of the dissolution test. The passive release was initially found to produce a controlled release kinetics, with a mean cumulative release of 69.75 ± 4.99 % at 30 min. The drug release from passive films presented initially with the slowest release kinetics, however, it gradually surpassed the release from samples subjected to negative voltages. Drug release from the passive samples indicated concentration gradient-mediated release from the electroactive films. The swelling ratio for the MB-loaded films was recorded as 53.3 ± 5.9 %, which may have also contributed to the burst release, especially for a hydrophilic molecule like MB.

To quantify the difference between the release profiles depicted in Fig. 4 (a), the f_2 similarity factor was calculated to compare all release profiles against one another (Table S1) [40]. With the exception of +0.5 vs +1.0 V and +0.5 vs −0.5 V, the f_2 similarity factor for all other comparisons was below 50, thus revealing that the majority of the samples exhibited a different release profile. At the end of 180 min, a statistically significant difference in release was observed between, −1.0, 0.0, and +1.0 V, which were 76.46 ± 5.48 %, 91.92 ± 1.54 % and 99.41 ± 0.34 %, respectively ($p < 0.05$). No significant difference was observed between 0 V and either ±0.5 V, which was confirmed by ANOVA ($p < 0.05$). Thus, applying ±1 V was needed to significantly alter the cumulative release after 180 min compared to passive release.

Furthermore, the pulsatile characteristics of the conductive elastomer were also investigated. The results depicted in Fig. 3 (d) confirmed that the PEDOT:PSS/TPU/MB films can maintain their conductivity for up to 100 CV cycles. Here, samples were cycled between "on" (1.0 V) for 2.5 min and "off" (0.0 V) for 5 min. Samples were found to instantaneously respond to the voltage, as evidenced by the sudden sharp rise in vertical peaks in the multi-amperometry sweep plot each time they were switched on (Fig. 4 (b)). The current constantly peaked at 6.25 ± 0.00 mA, which was followed by an exponential decrease to a steady-state of approximately 0.75 ± 0.03 mA. When the voltage was set to 0.0 V (i.e., switched off), a sudden sharp rise in the negative direction was observed, which was followed by an exponential increase in current towards a steady-state of 0.00 mA. As for drug release, the "on" cycle had a marked effect on the release kinetics. It was observed that the first "on" had the most pronounced effect, where the release kinetic substantially deviated from its normal trajectory, rapidly rising from 30 % to 68 % release. (Fig. 4 (c)). After switching off the voltage, the rate of release decreased, as evident by a decrease in the slope of the curve. Upon a second switching "on" of the voltage, a notable increase in the release slope was observed and similarly for when the voltage was switched "on" for a third time; both these "on" resulted in a less pronounced effect on the release profile compared to the first time the voltage was applied. Compared to the passive release, both sample sets initially presented with similar release kinetic, however, following the first stimuli, a difference in their release was observed. Overall, the conductive elastomer was confirmed to be electrically responsive to programmable pulsatile stimulus, and while all three pulses resulted in identical current responses, their effect on drug release varied between the first voltage pulse and the remaining two pulses.

Following the *in vitro* analysis, the mechanical properties of the films were investigated, with respect to tensile strength, elastic modulus and elongation at break (Fig. 4 (d)–(f)). Attempts were made to analyse PEDOT:PSS films, however, these films habitually fractured when clamped. Three samples were analysed, which were the PEDOT:PSS/TPU, PEDOT:PSS/TPU/MB and the PEDOT:PSS/TPU/MB after the *in vitro* analysis, following MB release. The analysis revealed that the addition of MB to the PEDOT:PSS/TPU films increased the mean tensile strength from 7.92 ± 1.92 MPa to 9.90 ± 1.00 MPa, while also increasing the elastic modulus from 173.65 ± 69.91 MPa to 418.95 ± 120.15 MPa. In contrast, the mean elongation at break decreased with the addition of MB, from 6.82 ± 2.79% to 4.67 ± 0.93%. Following the *in vitro* and MB release at +1.0 V, both the mean tensile strength and mean elastic modulus significantly decreased, to 3.07 ± 0.99 MPa and 33.67 ± 9.34 MPa, respectively; whereas the mean elongation at break was 6.26 ± 0.51 %. Therefore, the samples were found to weaken after the *in vitro* release, in regard to their strength and stiffness. The post-release films were visually inspected, however no defects were observed, and visually looked similar to their before release counterpart. SEM was then employed to reveal potential defects at the microstructural level, such as microfractures or pores that are known to negatively affect mechanical and structural properties [41–43]. However, no such common defects were observed (Fig. 4(g–i)). One notable observation was that films subjected to +1.0 V were presented with crystals on their surface (Fig. 4 (i)), which is believed to be due to PBS ions nucleating.

4. Discussion

The study is the first to 3D print a conductive elastomer with voltage-responsive drug release. We elucidated the effect of polymer loading and as a result, we were able to elucidate the optimal rheological characteristics needed for printing the conductive elastomer. The rheological properties were comparable to other DIW formulations, where printable inks have a G' between 10^1 to 10^5 Pa [44–51]. The rheological analysis revealed a similar trait to the work by Yuk et al. (2020), in that ostensibly minor increases in rheological characteristics resulted in under-extrusion [35]. Building on the study Yuk et al. we demonstrate that it is possible to blend PEDOT:PSS with up to 6 w/v% TPU and still obtain a conductive polymer. Recent work reported that such a blend is biocompatible, further justifying the use of polyurethane polymers [52].

Furthermore, we also demonstrate that the 3D printed conductive elastomers possess comparable mechanical properties to wearable devices [53,54], however the stretchability will need to be improved [55–57]. Consideration will also need to be given to the effect of drug loading the device. We observed a decrease in the elongation at break with the addition of MB, where the addition of a drug (or filler) to a polymeric device is known to reduce its flexibility [46,58]. Fortunately, this can be counteracted through the use of plasticizers [59,60]. Herein, the theoretical drug content in the device after solvent evaporation was ~9.1 w/w%. Increasing the drug loading content will expand the utility of the conductive elastomer as a DDS since it will be able to deliver more drug. The addition of TPU improved the mechanical properties of PEDOT:PSS films and despite being electrically insulating, the blended formulation was found to be conductive and sufficient to affect drug release via voltage control, despite a 67.54 % decrease in its peak current. Future work will seek to develop a device that is flexible yet with higher conductive properties, which we hypothesise in turn will improve the device's response to voltage.

Whilst 3D printing was used for its dimensional precision, we found it to rapidly accelerate the research. For one, 3D printing is fast and allowed for multiple samples to be simultaneously printed. In addition,

printing only the desired net structure expedited the drying phase. Had solvent casting been used then more time would have been needed for drying, due to a lower surface area. Moreover, solvent casting would have required an additional post-processing step of cutting the casted sheet into the desired shapes, which is both time and resource consuming. Producing the net shape with 3D printing overcame these issues, and thus accelerated the overall research. Thus, the combination of precision and sustainability revealed that 3D printing is suitable for emerging research policies [61–65].

Another novel finding was observed from analysing the films after the *in vitro* study. Despite the post-release sample expelling MB, the tensile strength and elastic modulus were significantly lower than films printed with PEDOT:PSS/TPU, which also contained no MB. The films were found to be more ductile, which is likely to be due to water entering the polymeric matrix and plasticising the films [66]. The conductive elastomer was able to release 100 % of its drug content without degrading, which suggests that it can potentially be re-used. The 100 CV cycle analysis and SEM images provide encouraging results that such a feat can be achieved. However, the mechanical properties following post-release require further investigation, with a view to finding a solution that allows the conductive elastomer to maintain its mechanical properties post-release. The main motivation for such a system would be in the interest of planetary health [67].

The impact of electroactive DDS is expected to go beyond controlled drug release. Healthcare is undergoing a digital revolution, where AI and digital techniques like 3D printing are providing rapid transformation [68–73]. However, there has been a lack of research dedicated to digitalising medicines. This can hinder advancements, as current solid dosage forms offer limited monitoring and automation. If medicines can be digitalised, then they can communicate with AI, which has been demonstrated to possess super-human speed and intelligence [74]. By digitalising medicines, through CPs for example, then we can achieve an integrated healthcare system, like the internet of things (IoT) framework, where all aspects of the medicine pipeline can seamlessly communicate with each other [75–78]. For example, AI can be the decision-maker; 3D printing can fabricate the desired medicine; and CPs can be used to monitor and actuate drug release [79,80]. In order to realise this aim, further cross-disciplinary research and expertise is needed.

Several challenges were overcome in this study, namely achieving a printable formulation that exhibits suitable mechanical and electrical properties and is capable of modulating drug release via voltage stimuli. Future work will seek to build on this to realise the potential of merging CPs with 3D printing. MB was used as a model drug and thus future work will seek to use clinically relevant drugs like dexamethasone to realise the potential of the platform for clinical applications [81]. While we demonstrate that our 3D printed device works with a positively charged drug, previous work has demonstrated that the system is compatible with both positively and negatively charged molecules [82]. However, the effect of negatively charged molecules on the extrusion process and their subsequent effect on the mechanical properties of the device will need to be elucidated. Further work will also need to investigate the electrical stability of the electroactive films as a function of time (e.g., 3, 6, 9 months). While 3D printing is a powerful rapid prototyping fabrication technique, there is a need to investigate the potential for scaling-up the technology. The evidence thus far is encouraging, as scaling up the size of the printed object was successfully demonstrated to maintain the same release rate [83]. However, 3D printing is not yet at the level of large-scale manufacturing due to its speed compared to current manufacturing technologies [84].

In addition, further work is needed to understand the mechanism behind the initial burst release when the films were subjected to a negative voltage (Fig. 4 (a)). It has been demonstrated that reversing the polarity does not completely prevent drug release, as observed herein [85–88]. This could be due to voltage-induced swelling [89], and thus requires further investigation. The pulsatile results warrant further investigation to understand the cause behind the varying release respond to the same voltage pulse (Fig. 4 (c)), albeit the results were comparable to previous work, in which the first pulse caused the largest pronounced effect [90–92]. If addressed, then there is potential to further modulate the 3D printed electroactive platform, thereby further widening its applicability. Furthermore, two key areas of interest will be to develop a platform that can accommodate neutrally charged drugs and improving the drug loading. There are several clinically relevant drugs that are neutrally charged, such as paracetamol, atorvastatin and carbamazepine [93], that will not respond to an electrical stimulus, thus limiting the clinical application of electroactive DDS. Therefore, there is a need to develop a solution that will allow neutrally-charged drugs to be compatible with electroactive DDS.The present study developed electroactive films that, in their current form, can be further investigated as transdermal patches or wound dressings, due to their 2D form. However, future work will seek to develop 3D electroactive structures to further expand the range of dosage forms, such as subcutaneous implants. Thereafter, there is potential to explore more innovative applications, such as self-healing DDS and self-powered DDS [94–98].

5. Conclusion

The present study successfully demonstrated the 3D printing of an electroactive DDS. As this was the first study into this platform, a thorough characterisation analysis was performed on both the inks and printed structures. PEDOT:PSS was blended with TPU to obtain a substrate with sound mechanical properties. A maximum of 6 w/v% TPU could be blended with 4 w/v% PEDOT:PSS, as higher polymer loadings were found to produce undesirable prints. Rheological analysis revealed that increasing either polymer resulted in an increase in G', and thus reaching viscosity values that rendered the inks difficult to print. While TPU was found to improve the mechanical properties of PEDOT:PSS, CV analysis revealed that the addition of TPU decreased the peak current by 67.54 %. Furthermore, 100 CV cycles revealed that the peak current of PEDOT:PSS/TPU/MB films decreased with increasing cycles, by up to 19.30 %. *in vitro* drug release revealed that varying the voltage from −1.0 to +1.0 V can modulate drug release, which was quantified using the f_2 similarity factor. Furthermore, we demonstrated that the films can electrically respond to pulsatile voltages, which consequently was found to alter its release profile. Mechanical analysis revealed that post-release films were mechanically weaker than as-printed films. The results reveal that more work is needed to improve what is potentially a revolutionary platform.

CRediT authorship contribution statement

Manal E. Alkahtani: Writing – original draft, Visualization, Project administration, Methodology, Investigation, Formal analysis, Data curation, Conceptualization. **Siyuan Sun:** Writing – original draft, Visualization, Investigation, Data curation. **Christopher A.R. Chapman:** Writing – review & editing, Supervision, Methodology, Formal analysis, Conceptualization. **Simon Gaisford:** Writing – review & editing, Supervision, Resources, Funding acquisition. **Mine Orlu:** Writing – review & editing, Resources, Funding acquisition. **Moe Elbadawi:** Writing – review & editing, Writing – original draft, Supervision, Methodology, Investigation, Formal analysis, Data curation, Conceptualization. **Abdul W. Basit:** Writing – review & editing, Supervision, Resources, Funding acquisition.

Declaration of competing interest

The authors declare that they have no known competing financial interests or personal relationships that could have appeared to influence the work reported in this paper.

Data availability

Data will be made available on request.

Acknowledgments

The authors would like to thank Prince Sattam bin Abdulaziz University, Alkharj, Saudi Arabia, for their financial support of Manal E. Alkahtani through the Postgraduate Research Grant. M.E. would like to acknowledge the Engineering Physical Science Research Council for their funding support [Grant number: EP/S009000/1].

Appendix A. Supplementary data

Supplementary data to this article can be found online at https://doi.org/10.1016/j.mtadv.2024.100509.

References

[1] M.T. Manzari, et al., Nat. Rev. Mater. 6 (4) (2021) 351.
[2] S.M. Mirvakili, R. Langer, Nature Electronics 4 (7) (2021) 464.
[3] S. Hosseini, Smart Drug Delivery Systems: Concepts and Clinical Applications, 2021.
[4] Y. Park, et al., Appl. Sci. 9 (6) (2019) 1070.
[5] Palza, H., et al., (2019) 12 (2), 277.
[6] P. Makvandi, et al., Mater. Today 47 (2021) 206.
[7] M. Zhang, et al., Materials Today Bio 14 (2022) 100223.
[8] B. Tandon, et al., Adv. Drug Deliv. Rev. 129 (2018) 148.
[9] S. Paramshetti, et al., Pharmaceutics 15 (4) (2023) 1204.
[10] C.A.R. Chapman, et al., Appl. Phys. Lett. 116 (1) (2020) 10501.
[11] Saberi, A., et al., (2019) 9 (9), 448.
[12] Park, Y., et al., (2019) 9 (6), 1070.
[13] M. Criado-Gonzalez, et al., ACS Appl. Polym. Mater. 3 (6) (2021) 2865.
[14] Lucía Rodríguez-Pombo, María José de Castro-López, Paula Sánchez-Pintos, Jose Maria Giraldez-Montero, Patricija Januskaite, Goretti Duran-Piñeiro, M. Dolores Bóveda, et al., "Paediatric clinical study of 3D printed personalised medicines for rare metabolic disorders.", International Journal of Pharmaceutics 657 (2024) 124140.
[15] E. Mathew, et al., Pharmaceutics 12 (3) (2020) 266.
[16] Seoane-Viaño, I., et al., (2021).
[17] M.A. Ali, et al., Adv. Funct. Mater. 32 (9) (2022) 2270057.
[18] Y.J.N. Tan, et al., Int. J. Pharm. 598 (2021) 120370.
[19] M. Siyawamwaya, et al., Eur. J. Pharm. Biopharm. 138 (2019) 99.
[20] Y. Cheng, et al., Int. J. Pharm. 591 (2020) 119983.
[21] M. Kyobula, et al., J. Contr. Release 261 (2017) 207.
[22] J. Zhang, et al., Carbohydr. Polym. 177 (2017) 49.
[23] Goyanes, A., et al., (2015).
[24] I. Koutsamanis, et al., J. Contr. Release 335 (2021) 290.
[25] Robles-Martinez, P., et al., (2019).
[26] S.A. Khaled, et al., J. Contr. Release 217 (2015) 308.
[27] C.S. O'Reilly, et al., Pharmaceutics 13 (12) (2021) 2187.
[28] N. Allahham, et al., Pharmaceutics 12 (2) (2020) 110.
[29] Kopp, Sebastian-Paul, Vadim Medvedev, Katja Tangermann-Gerk, Natalie Wöltinger, Richard Rothfelder, Fabian Graßl, Markus R. Heinrich, et al., "Electrophotographic 3D printing of pharmaceutical films.", Additive Manufacturing 73 (1–2) (2023) 103707.
[30] S.A. Sánchez-Guirales, et al., Pharmaceutics 13 (10) (2021) 1583.
[31] A. Awad, et al., Pharmaceutics 11 (4) (2019) 148.
[32] A. Goyanes, et al., Int. J. Pharm. 567 (2019) 118497.
[33] Rodríguez-Pombo, L., et al., (2022).
[34] P. Paixão, et al., Eur. J. Pharm. Biopharm. 112 (2017) 67.
[35] H. Yuk, et al., Nat. Commun. 11 (1) (2020) 1604.
[36] C.T. Cesco, et al., Pharmaceutics 13 (6) (2021) 842.
[37] X. Xu, et al., J. Nanobiotechnol. 20 (1) (2022) 297.
[38] T. Rager, et al., Phys. Chem. Chem. Phys. 14 (22) (2012) 8074.
[39] A. Farmoudeh, et al., Drug Delivery and Translational Research 10 (5) (2020) 1428.
[40] J.W. Moore, H.H. Flanner, Pharmaceut. Technol. 20 (1996) 64.
[41] X. Wang, et al., Polymers 11 (7) (2019) 1154.
[42] C. Valenzuela, et al., LWT - Food Sci. Technol. (Lebensmittel-Wissenschaft -Technol.) 50 (2) (2013) 531.
[43] R. Balint, et al., Acta Biomater. 10 (6) (2014) 2341.
[44] Z. Hou, et al., Frontiers in Materials 8 (2021).
[45] J. Zhao, et al., Adv. Funct. Mater. 29 (26) (2019) 1900809.
[46] M. Elbadawi, et al., Int. J. Pharm. 595 (2021) 120197.
[47] Q. Chen, et al., J. Hazard Mater. 427 (2022) 128190.
[48] S.-S. Lee, et al., Adv. Funct. Mater. 32 (34) (2022) 2202901.
[49] G. Shi, et al., Appl. Mater. Today 16 (2019) 482.
[50] T. Wu, et al., Mater. Des. 180 (2019) 107947.
[51] C.M. Larson, et al., Adv. Eng. Mater. 18 (1) (2016) 39.
[52] E. Cuttaz, et al., Biomater. Sci. 7 (4) (2019) 1372.
[53] V. Jain, et al., Microsystems & Nanoengineering 5 (1) (2019) 29.
[54] L. Wang, et al., Chem. Eng. J. 455 (2023) 140609.
[55] X. Wang, et al., Nano-Micro Lett. 13 (1) (2021) 64.
[56] H.C. Ates, et al., Nat. Rev. Mater. 7 (11) (2022) 887.
[57] Y. Wu, et al., Mater. Chem. Front. 7 (16) (2023) 3278.
[58] L.M. Schmidt, et al., Int. J. Pharm. 620 (2022) 121750.
[59] E.M. Maher, et al., Drug Deliv. 23 (8) (2016) 3088.
[60] P. Jantrawut, et al., Polymers 9 (7) (2017) 289.
[61] B. Haibe-Kains, et al., Nature 586 (7829) (2020) E14.
[62] H. Li, et al., Int. J. Pharm. 648 (2023) 123561.
[63] A. Oza, Nature (London) 622 (7984) (2023) 677.
[64] NewsRx Health & Science, 2019, p. 218.
[65] S. Sun, et al., Pharmaceutics 15 (11) (2023) 2630.
[66] D.-H. Xu, et al., Polymer 218 (2021) 123498.
[67] M. Elbadawi, et al., Int. J. Pharm. 639 (2023) 122926.
[68] L.K. Vora, et al., Pharmaceutics 15 (7) (2023) 1916.
[69] Elbadawi, M., et al., (2021).
[70] I. Seoane-Viaño, et al., Adv. Drug Deliv. Rev. 174 (2021) 553.
[71] S.J. Trenfield, et al., Expet Opin. Drug Deliv. 16 (10) (2019) 1081.
[72] D. Kumar Gupta, et al., J. Drug Target. 30 (2) (2022) 131.
[73] M. Elbadawi, et al., Appl. Mater. Today 36 (2024) 102061.
[74] E. Kaufmann, et al., Nature 620 (7976) (2023) 982.
[75] L.M. Dang, et al., Electronics 8 (7) (2019) 768.
[76] A. Kishor, C. Chakraborty, Wireless Pers. Commun. 127 (2) (2022) 1615.
[77] S. Zeadally, O. Bello, Internet of Things 14 (2021) 100074.
[78] S.J. Trenfield, et al., Adv. Drug Deliv. Rev. 182 (2022) 114098.
[79] F. Ghorbani Zamani, et al., TrAC, Trends Anal. Chem. 118 (2019) 264.
[80] M.E. Alkahtani, et al., Advanced Healthcare Materials, 2023 e2301759.
[81] C. Kleber, et al., Adv. Healthcare Mater. 8 (10) (2019) 1801488.
[82] C.A.R. Chapman, et al., Materials Today Bio 23 (2023) 100883.
[83] J.H. Teoh, et al., J. Contr. Release 341 (2022) 80.
[84] A. Geraili, et al., VIEW 2 (5) (2021) 20200126.
[85] C.J. Pérez-Martínez, et al., React. Funct. Polym. 100 (2016) 12.
[86] M. Bansal, et al., Acta Biomater. 137 (2022) 124.
[87] M. Zhu, et al., RSC Adv. 9 (22) (2019) 12667.
[88] A.M. Orduño Rodríguez, et al., Polym. Bull. 77 (3) (2020) 1217.
[89] M. Modarresi, et al., Macromolecules 53 (15) (2020) 6267.
[90] D. Aycan, et al., Int. J. Biol. Macromol. 231 (2023) 123297.
[91] J. Qu, et al., Int. J. Biol. Macromol. 140 (2019) 255.
[92] M. Bansal, et al., J. Contr. Release 328 (2020) 192.
[93] J. Trognon, et al., Sci. Total Environ. 912 (2024) 169040.
[94] Y. Li, et al., Adv. Funct. Mater. 30 (30) (2020) 2002853.
[95] X. Xin, et al., Synth. Met. 268 (2020) 116503.
[96] D. Rybak, et al., J. Mater. Chem. B 12 (7) (2024) 1905.
[97] N. Wen, et al., Nano Energy 78 (2020) 105361.
[98] C. Xu, et al., Compos. Commun. 32 (2022) 101179.